RSC Advances

REVIEW

View Article Online
View Journal | View Issue

Cite this: *RSC Adv.*, 2024, **14**, 28927

Carbon nanomaterials as electrochemical sensors for theophylline: a review

Laurencia Gabrielle Sutanto,[a] Syarifa Sabilla,[a] Brasstira Yuva Wardhana,[a] Anggi Ramadani,[a] Anis Puspita Sari,[b] Qonita Kurnia Anjani,[c] Wan Jeffrey Basirun, [de] Tahta Amrillah, [a] Ilma Amalina [a] and Prastika Krisma Jiwanti *[a]

Received 16th May 2024
Accepted 26th July 2024

DOI: 10.1039/d4ra03585b

rsc.li/rsc-advances

Theophylline (TP) is a methylxanthine derivative, which serves as a valuable compound in treating respiratory disorders and acts as a bronchodilator agent. However, TP has a limited therapeutic range (20–100 μmol L^{-1}), demanding precise monitoring to prevent potential drug toxicity even with slight level fluctuations during treatment. Thus, to overcome this limitation, electrochemical methods have been extensively used due to their efficacy in achieving sensitivity, selectivity, and accuracy. In the context of electrochemical sensors, nanocarbon-based materials have gained widespread recognition for their extensive applications. Therefore, this review aims to explore the latest advancements in carbon-based electrodes particularly used for the precise determination of TP through electrochemical methods. The results are expected to provide insights into the profound significance of the methods in enhancing the accuracy and sensitivity for the detection of TP.

Introduction

Theophylline (1,3-dimethyl-7*H*-purine-2,6-dione, TP) is a bronchodilator that belongs to the class of drugs known as methylxanthines (Fig. 1). This drug has been widely used for over 70 years to treat respiratory conditions, including asthma and chronic obstructive pulmonary disease (COPD). In addition, it is preferably used to treat bradycardia and apnea in premature newborns due to its effectiveness.[1,2] The mechanism of action of TP is associated with relaxing the smooth muscles in the airways, which helps to widen the air passages and improve breathing. TP is often available in various formulations, including tablets, capsules, and extended-release forms. Several studies have also shown that it is typically taken orally and its dosage may vary depending on the individual's condition and response. TP can be classified as a drug with a narrow therapeutic window of 20–100 μmol L^{-1}, which can cause toxicity at levels slightly above the therapeutic range. Excessive intake has been reported to cause certain side effects, such as nausea, vomiting, headaches, rapid heartbeat, as well as seizures in severe cases. Therefore, it is important to monitor the TP level for the treatment duration to avoid drug toxicity. In this case, blood tests may be periodically carried out to monitor the level of TP in the blood, as maintaining the proper therapeutic range is important for both safety and effectiveness.

In line with these findings, it is necessary to develop simple yet sensitive sensing devices to analyse TP in the human body. The current clinical practice for TP monitoring requires regularly taking blood samples from patients (nearly 25 mL or more is required), which is a challenge due to the high volume required. However, TP still has to be monitored using various techniques due to its toxicological effects. Thus, to overcome this challenge, certain methods have been developed, such as using high-performance liquid chromatography (HPLC),[3–5]

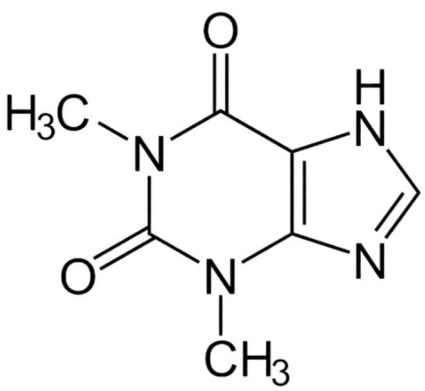

Fig. 1 Structure of theophylline.

[a]*Nanotechnology Engineering, Faculty of Advanced Technology and Multidiscipline, Universitas Airlangga, Surabaya 60115, Indonesia. E-mail: prastika.krisma@ftmm.unair.ac.id*

[b]*Department of Chemistry, Faculty of Science and Technology, Universitas Airlangga, Surabaya 60115, Indonesia*

[c]*School of Pharmacy, Medical Biology Centre, Queen's University Belfast, 97 Lisburn Road, Belfast BT9 7BL, UK*

[d]*Nanotechnology and Catalysis Research Center (NANOCAT), University Malaya, Kuala Lumpur 50603, Malaysia*

[e]*Department of Chemistry, Faculty of Science, University Malaya, Kuala Lumpur 50603, Malaysia*

spectrophotometry,[6] immunosorbent surface,[7,8] and colorimetry.[8] However, despite their potential, there is still a lack of efficiency due to various factors, such as prolonged preparation, the need for a trained technician to operate the machine, and high costs. Consequently, several studies have proposed the use of electrochemical methods, which are effective and have various benefits, including sensitivity, selectivity, easy operation, cost-effectiveness, and miniaturization.[9–11]

To achieve a highly reliable, accurate, and stable electrochemical sensor system, careful consideration and choice of the working electrode is crucial. The electrode is the component that directly comes into contact with the sample, playing a critical role in determining the performance of the method. This indicates that selecting an appropriate material by considering the design and conditioning can significantly improve the quality and robustness.

Metal-type electrodes have been reported to have the benefit of possessing high catalytic activity but a narrow potential window and high background current. Meanwhile, carbon-based electrodes have the advantage of stability, relatively wide potential window, low cost, and ability to be functionalized.[12,13] To improve the accuracy of the electrochemical method for the determination of TP, it is necessary to overcome the limitation of positive oxidation potentials. This can be achieved using a wider potential window electrode to prevent interference from background currents. The selection of an appropriate electrode material is important, which must meet the required properties, such as stability, cost-effectiveness, and large surface area. Optimization of the material is also essential to achieve reliable TP detection and prevent interference.[14–16]

In this review, the recent advancements in nanocarbon-based electrodes, such as graphene, carbon nanotubes (CNTs), and nanodiamonds (NDs), for the determination of TP using the electroanalytical method are discussed. The bare carbon-based electrode and its functionalized variants are discussed in terms of their sensitivity, limit of detection (LOD), selectivity, and application in real samples. The results are expected to provide a comprehensive view to readers about the new trend of TP determination together with the future prospect of TP sensors using the electroanalytical method.

Carbon nanomaterials

Nanomaterials have attracted a lot of interest due to their properties and features, which are absent in other materials. Carbon nanomaterials (CNM) have the potential to be used in various fields because of their unique properties and characteristics with widespread application. The properties of CNM are highly dependent on their structure, shape, size, and dimensions. The CNM considered in this review are NDs (3-dimensional nanomaterials), graphene and its derivatives (2-dimensional nanomaterials), CNTs (one-dimensional nanomaterials), and fullerenes and quantum dots (zero-dimensional nanomaterials), as shown in Scheme 1.[17] In general, CNM have various advantages, such as high electrical conductivity, mechanical resistance, strong physical and chemical stability,

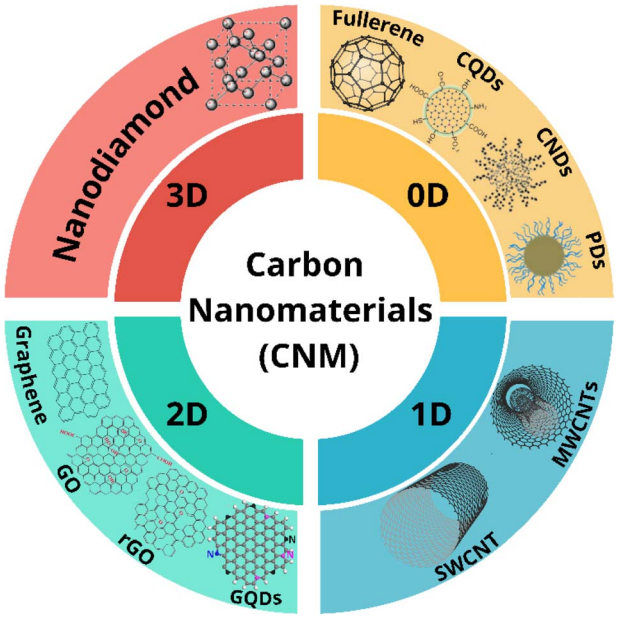

Scheme 1 Various forms of CNM including 0D, 1D, 2D, and 3D carbon nanostructures.

excellent electronic properties, large thermal conductivity, transparency, and wide surface area.[18–21]

Graphene is a 2-dimensional carbon allotrope nanomaterial with one-atom thickness.[22] The structure of graphene is comprised of a layer of sp^2-bonded carbon atoms arranged in a honeycomb motif.[23,24] Currently, this material is gaining attention because it has interesting properties, such as outstanding electronic transport properties, wide surface area, high thermal conductivity, chemical inertness, optical transmittance, and high hydrophobicity.[22,23] Graphene-based nanomaterials have great potential as biosensing materials due to their wide surface area, high electrical conductivity, optical properties, excellent binding capacity with biomolecules, and easy modification. Additionally, these materials have outstanding biocompatibility with low toxicity.[22] Graphene can be synthesized by exfoliating a layer of graphite into a single layer. However, there are some challenges in the synthesis of graphene, such as the creation of defects in the surface of graphene sheets during their preparation, difficulty, time-consuming, and very low yields.[25] Graphene also has poor solubility and agglomeration in solution due to the presence of van der Waals interactions.[26] The family of graphene-based materials has many members, such as graphene oxide (GO), reduced graphene oxide (rGO), and graphene quantum dots (GQDs).

Among them, GO is a one-atom-thick nanostructured material produced by the oxidation of graphene sheets[27] and has several oxidized aromatic C=C double bonds. In addition, it possesses different functional groups, namely hydroxyl, epoxy, carbonyl, and carboxyl groups.[28,29] Compared to graphene, GO has several functional groups that can increase its solubility in water and polar solvents, endowing it with hydrophilic properties due to the presence of hydroxyl and epoxy groups.[28] The

presence of these functional groups allows GO to easily exfoliate in water or other solvents to produce a stable dispersion.[30] This sensor has many advantages because it is easily obtained by the chemical oxidation of graphite, has a 2-dimensional structure with a very high surface area, is cost-effective, easy to synthesize, and has thermal and chemical stability.[31] GO also exhibits high stability and is commonly used as a support in composites and to stabilize many nanoparticles, such as Au, ZnO, MnO_2, TiO_2, and Fe_3O_4. This is due to the numerous functional groups (–OH, C–O–C, and –COOH) on the surface of GO, which provide reactive sites for the binding of metal nanoparticles. Thus, GO can be applied in various fields, for example, its stability in the electrochemical sensor field is demonstrated by its detection performance during repeated measurements on the same sample. Previous studies have shown that the stability of GO maintained a peak current response that did not significantly differ from the initial response.[32] This indicates that GO had high stability when tested as an electrochemical sensor. However, despite its many advantages, GO also has a weakness, namely, its conductivity is lower compared to graphene.[33]

rGO is a graphene-derived nanomaterial made by exfoliating graphite into graphene oxide and reducing it to reduced graphene oxide.[34] When it is reduced, the rGO material is produced, where most of the sp^3 oxygen and carbon groups are removed to obtain a material that looked more like graphene but with much better properties.[35,36] Some of the methods for the synthesis of rGO from GO are thermal (photothermal), chemical (photochemical), microwave, and different bacterial methods as well as using microbes by reducing the amount of oxygen.[29,35] rGO has several interesting properties such as excellent electrocatalytic properties, wide surface area, high electrical conductivity, mechanical strength, and biocompatibility.[37] Due to the properties of rGO, it has potential to be applied in the fields of electronic devices, energy storage and conversion, sensors, and composites.[38,39] However, rGO tends to agglomerate irreversibly through its van der Waals bonds, leading to a decrease in its surface area.[38]

GQDs are graphene derivatives that possess quantum confinement and nanoscale graphene edge effects.[30] GQDs are known as zero-dimensional nanomaterials with unique properties such as optical, electrical, electronic, fluorescent, photoluminescent, and optoelectronic properties.[40,41] GQDs are a type of carbon quantum dots (CQDs) derived from graphene or GO. Also, they are small graphene sheets with lateral dimensions smaller than 100 nm and less than 10 layers thick.[41] GQDs are considered a new type of quantum dots (QDs) with reliable chemical and physical stable properties, environmentally friendly nature due to their non-toxicity and characteristics of being biologically inert with stable fluorescence, high conductivity, luminescence, high solubility, biocompatibility, and adjustable bandgap.[35,40,41] Thus, due to the characteristics of GQDs, they have the potential to be applied in various fields such as solar cells, bioimaging, batteries, photoelectrocatalysis, and sensors.[39]

CNTs are another interesting type of carbon material, which form one-dimensional carbon nanostructures. CNTs consist of carbon atoms arranged in a series of benzene rings coiled into a cylindrical shape.[42] CNTs are nanomaterials made of sheets of hexagonal carbon atoms (graphene) with nanometer dimensions and hollow structures.[43,44] CNTs possess sp^2 bonds, which endow them with excellent mechanical properties, and CNTs are considered the strongest materials.[45] Furthermore, they have several advantages such as high thermal conductivity, flexibility, and elasticity because they can bend, twist, and return to their original shape, while maintaining their properties, outstanding electronic properties, and high electrical conductivity.[44,46,47] Thus, due to these superior characteristics, CNTs have the potential to be applied in the fields of batteries,[48] solar cells,[49] hydrogen storage,[50] and chemical sensors.[51] However, CNTs have poor solubility in water and organic solvents, which can usually be overcome through their functionalization.[44,52]

CNTs can be classified into 2 categories including single-walled carbon nanotubes (SWCNTs) and multi-walled carbon nanotubes (MWCNTs).[42] SWCNTs are sp^2 hybridized carbon with a hexagonal structure coiled to form a hollow tube with a diameter of 0.4–2 nm.[52] Meanwhile, MWCNTs were concentric cylinders consisting of 2 or more graphene layers coiled with an outer diameter of several nanometers to more than 10 nm with a distance between layers of 0.34–0.39 nm.[43,44] Both types of CNTs have high thermal conductivity, namely 3500 W m^{-1} K^{-1} and more than 3000 W m^{-1} K^{-1} for SWCNT and MWCNTs, respectively.[44]

3D nanostructured carbon has been extensively investigated as a diamond material, which is a metastable allotrope nanomaterial of carbon with the carbon atoms arranged to for a face-centered cubic crystal structure.[53] Metastable is a condition in which a material is unstable and can change into a more stable or less stable state. However, diamonds are metastable under ambient conditions, and in the absence of oxygen, water, or other reagents, bulk diamonds are believed to be stable against graphitization below 1800 K at zero pressure.[54] Structurally, pure and perfect diamonds are colorless and transparent.[55] NDs are nanoscale diamonds, which possess a complex structure in the form of a sphere consisting of a diamond core with an outer shell of graphite carbon containing many oxygens functional groups on its outer surface.[53,56] Due to the presence of these oxygen functional group, ND particles are hydrophilic. In addition, the graphite shell present on the outer surface of NDs has sp^2 hybridization, which can provide surface chemistry and enable further functionalization.[57] NDs are spherical with an average diameter of 5 nm with a very narrow size distribution and wide surface area. A unique chemical property of NDs is that their surface is mostly covered with abundant carboxyl, hydroxyl, ketone, ether, pyrene, and sulfonic acid groups.[56,57] This material possesses outstanding mechanical and optical properties, thermal stability, large surface area, high thermal conductivity, fluorescence properties from its diamond core, and biocompatibility, and is chemically inert because it is mostly composed of sp^3 hybridized carbon atoms.[53,55,58] Thus, based on their properties and advantages, NDs can be applied in various fields such as photocatalysis,[59] electrochemical sensors,[60] biomedicine, and cosmetics.[61]

Fullerenes are a type of carbon allotrope with dimensions of 0 and a closed cage ball structure (buckyball) featuring pentagonal and hexagonal patterns.[62–64] The presence of pentagons in the structure of fullerenes results in the formation of curvatures and closure of structures similar to cages.[65] Fullerenes are represented by the C_{2n} notation, where $n \geq 10$, which are known to exist in various forms such as C_{60}, C_{70}, C_{76}, C_{82}, and C_{84}. However, typically only C_{60} and C_{70} have been extensively investigated.[63,65] The C_{60} molecule has a cage structure consisting of 60 sp^2 hybridized carbon atoms with each cage containing 12 pentagons and 20 hexagons.[62] C_{60} possesses 2 types of C–C bonds, namely single bonds and double bonds. In the pentagonal rings, there is only one single bond, while in the hexagonal rings there are alternating single and double bonds. The ribs between the pentagon and hexagon rings are single bonds, and the ribs between the 2 hexagon rings are double bonds. The average length of a single bond is 0.145 nm and that of a double bond is 0.141 nm.[66] C_{60} fullerenes have many advantages such as high electronegativity and they can accept a large number of electrons, resulting in efficient electron transfer, high sensitivity, physical and chemical stability, improved conductivity, charge transfer, a narrow bandgap, and a unique structure, which guarantees minimal changes in their structure.[63,65–67] However, fullerenes have several limitations such as low solubility in water, easy agglomeration, low dispersibility, tendency to degrade or decompose in the presence of light and oxygen, and high cost.[64,66,67] Based on their properties and advantages, fullerenes can be applied in various fields such as photovoltaics and photocatalysts due to their narrow bandgap electron and energy transfer process,[63,66] in the cosmetic field, namely anti-aging because of their nature in counteracting radicals,[68] in the field of sensors due to their high electrical conductivity and load-transport properties,[65] and batteries, solar cells, drug delivery,[66] and catalysts.[64]

QDs are zero-dimensional carbon-based materials, measuring 2–10 nm and containing 10–50 atoms in quantum volume.[69] They are members of the family of QDs, namely CQDs, GQDs, carbon nanodots (CNDs), and polymer dots (PDs). CQDs are often referred to as carbon dots, which are carbon-based nanomaterials that are members of the family of QDs. They are zero-dimensional nanomaterials with a very small size and relatively strong fluorescence characteristics,[70] which have attracted significant attention because of their excellent chemical stability, high conductivity and water solubility, photoluminescence properties, broadband optical absorption, superior photostability, resistance to photobleaching, low toxicity, easy functionalization, and biocompatibility.[41,70] However, compared to GQDs, CQDs usually show poorer crystallinity and more defects, with a lower crystalline sp^2 carbon content. Thus, considering their properties and unique characteristics, CQDs can be applied in various fields such as biomedicine, catalysts, energy, photoelectronic applications, and sensing.[41] However, among the family of QDs, this nanomaterial has a size of less than 10 nm. CNDs usually contain many functional groups at their edges, such as carboxyl, hydroxyl, carbonyl, and epoxide, which are useful as reaction sites.[71] Also, they have attracted attention due to their excellent optical properties, low photobleaching, unique biocompatibility, superior chemical inertness and solubility, high electrical conductivity, large active area, and low toxicity.[71,72] Due to these remarkable properties, CNDs have been applied in the fields of bioimaging, solid-state lightening, and chemical sensing.[72] Besides CQDs, GQDs, and CNDs, PDs are also nanomaterials belonging to the QD family. PDs are aggregate polymers or crosslinks made of linear polymers or monomers. Carbon nuclei and connected polymer chains can self-assemble to form PDs. PDs are very promising as fluorescent materials and have excellent biocompatibility properties and low cytotoxicity.[73]

Bronchodilator drugs

Bronchodilators are drugs that are specifically designed to treat bronchoconstriction, which refers to the narrowing of the bronchial airways. Bronchodilators work by relaxing the muscles of the bronchi (airways) in the lungs. The pharmacological effects of bronchodilators facilitate increased airflow dynamics, thereby increasing the ease of breathing.[74] When the airways expand, it becomes easier to expel mucus, and thus bronchodilators facilitate the cleaning of mucus in the pulmonary system, where one way is through the coughing process.[75] These drugs are often administered to patients who are experiencing difficulty breathing or lung hyperinflation, such as asthma and COPD.[76] Thus, bronchodilators are important medications in the management of respiratory conditions and shown to have a significant impact on patient outcomes. Presently, there are 3 types of commonly used bronchodilator drugs, namely anticholinergics, TP, and long-acting beta2 agonists such as formoterol and salmeterol.

Beta-2 agonists

Beta-2 agonists are drugs that cause the smooth muscles surrounding the airways to relax by stimulating the beta-adrenoceptors in the airways, which have 2 main categories. The first type, known as short-acting beta-2 agonists (SABA), works to quickly widen the airways, while the second type, long-acting beta-2 agonists (LABA), helps to keep the airways open over an extended period. Albuterol is a type of SABA bronchodilator drugs. It helps to clear pulmonary edema fluid from the alveolus by accelerating the resorption of alveolar fluid.[77] In the study by J. Perez-Garcia *et al.* (2023), they reported that the use of albuterol has potential for substantial advancements in precision medicine for treating respiratory ailments.[78] This was achieved through the identification of epigenetic markers in whole blood that are linked to the response of bronchodilator drugs. This investigation indicated the involvement of DNA methylation in influencing the efficacy of bronchodilator therapy. These findings can be beneficial in categorizing treatment responses among pediatric asthma patients, enabling healthcare professionals to tailor asthma treatment and enhance patient outcomes.

Bronchodilator drugs, such as methacholine and salbutamol, have been found to be influenced by bronchial thermoplasty.[79] However, it is important to note that the response to

these drugs varied in different studies. For example, in the study by Goorsenberg *et al.* (2021), they reported a reduction in the response to methacholine with thermoplasty,[80] while in another study by Langton *et al.* (2018), they did not observe any significant effect. This inconsistency in the response was attributed to the limitations of spirometry monitoring, which lacked the sensitivity to assess the contribution of smooth muscle to the lung mechanics.[81] Consequently, a study employing oscillometry to evaluate the impact of thermoplasty on the bronchodilator response was conducted, leading to the conclusion that thermoplasty diminished the response to bronchodilator drugs.[82]

Beta-2 agonist drugs have several advantages in the treatment of obstructive lung diseases such as asthma and COPD.[83] The extended effectiveness of these drugs can be attributed to multiple factors, including the presence numerous side chains in their molecular structure. These side chains enhance the lipophilicity of the drug, increasing its retention in the lipid bilayer of the cell membrane.[77] However, there are some potential disadvantages and risks associated with their use. Studies reported that the activation of beta-2 receptors can increase the risk of arrhythmias, especially in patients with underlying cardiovascular disease.[84] Additionally, inhaling beta-2 agonists can acutely worsen hypoxemia, and the excessive use of these drugs can lead to reduced effectiveness over time and an increased likelihood of adverse effects such as tremors, tachycardia, and hypokalemia.[85,86]

Anticholinergic drugs

Anticholinergic drugs inhibit the effects of acetylcholine, a neurotransmitter responsible for triggering the contraction of airway muscles.[87] Through this inhibition, anticholinergics promote the relaxation of the airway muscles, thereby maintaining the openness of the airways. These medications have been alternatively termed muscarinic receptor antagonists due to their binding affinity for muscarinic receptors. Similar to beta-2 agonists, these drugs can be classified into 2 primary categories, including short-acting muscarinic antagonists (SAMA), such as tiotropium, and long-acting muscarinic antagonists (LAMA), which include medications such as aclidinium, glycopyrrolate, and umeclidinium.[77]

In the literature, a report demonstrated a bidirectional association between COPD-related comorbidities and cardiovascular conditions.[88] Consequently, individuals with cardiovascular ailments, particularly of an ischemic nature, require an evaluation through pulmonary function tests, such as spirometry.[76] Through observational study, drug therapy using the LABA–LAMA combination was reported to have a beneficial impact on the cardiovascular system in COPD,[89] and the maintained drug treatments were linked to alterations in the size of the left atrium. Moreover, Hohlfeld *et al.* (2018) studied lung deflation using bronchodilator drugs and concluded that a combination of LABA–LAMA (indacaterol–glycopyrronium) medications showed positive effects on the heart function of cardiovascular impairment in COPD.[90] A separate investigation was conducted to optimize the dosage ratios of bronchodilators to enhance synergistic combination therapy.[91] This study utilized isolated guinea pig tracheal rings to explore the pharmacological interplay between LABA–LAMA drugs. The findings of this study indicated that when administered at low doses, LABA and LAMA exhibited antagonistic interactions. Accordingly, the report proposed that large doses of both LABA and LAMA may be necessary to attain a synergistic interaction between these 2 drugs.

Anticholinergic medications have been shown to have no adverse effects on mucus clearance or viscosity and can even enhance mucus clearance by mitigating bronchoconstriction and airway inflammation.[77] However, there are certain potential drawbacks linked to their usage. The most prevalent side effects of inhaled anticholinergics stem from reduced vagal tone, leading to symptoms such as dry mouth, urinary retention, tachycardia, constipation, and gastrointestinal discomfort.[92] Also, it is worth noting that caution is warranted in elderly patients due to the potential for anticholinergics to induce delirium.[93] Additionally, reports suggest that prolonged use of anticholinergic drugs can result in changes in the brain, which bear a partial resemblance to that found in dementia or Alzheimer's disease.[94,95] Studies indicated that the anticholinergic properties impact functional rehabilitation in a range of conditions, spanning from more severe ailments such as stroke[96] to apparently minor injuries such as ankle sprains.[86]

Theophylline

TP is an easily accessible and cost-effective bronchodilator medication widely employed in the management of respiratory conditions, as shown in Scheme 2.[97] TP functions by relaxing the smooth muscles in the airways through the inhibition of phosphodiesterase (PDE). Furthermore, it has the potential to activate histone deacetyltransferases (HDACs), playing a role in its anti-inflammatory characteristics.[98] Thus, it can serve as an adenosine receptor antagonist, which is attributed to its capability to induce relaxation in the pulmonary vasculature.[99]

TP, an active pharmaceutical ingredient from the xanthine family, shares a close connection with plant alkaloids and exhibits unique biological and pharmacological properties. Additionally, it was reported that co-crystals of theophylline resorcinol monohydrate (THR) and theophylline pyrogallol monohydrate (THPY) have potential to amplify the effectiveness of medications, leading to a reduction in their adverse effects.[100] These co-crystals demonstrated strong inhibitory activity against pathogenic strains of *Streptococcus pneumoniae*, underscoring their antibacterial properties. Furthermore, the study by Rolta *et al.* indicated that among the methylxanthine drugs, TP demonstrated the highest binding affinity to all 3 target proteins of SARS-CoV-2, including the spike protein, main protease, and nucleocapsid protein. This discovery paved the way for potential future investigations into the role of theophylline as an antiviral treatment for COVID-19.[101]

TP, an established pharmaceutical agent with enduring prominence in its drug category, is conventionally recognized as a non-specific inhibitor of PDE. This attribute is associated with its moderate bronchodilatory effects and a wide array of

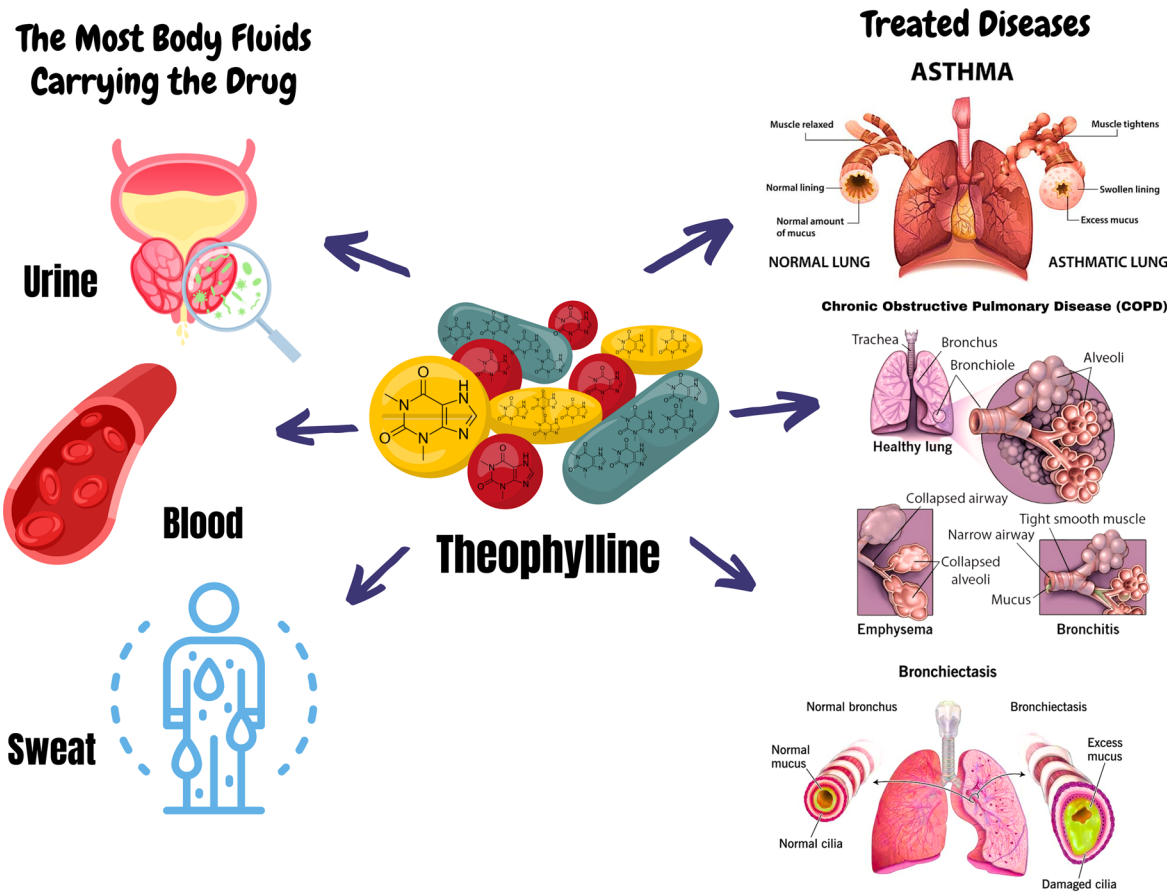

Scheme 2 Some respiratory diseases are treated using TP and body fluids containing drug residues.

undesirable side effects.[74] Consequently, to mitigate the side effects of this medication, it is imperative to implement measures to monitor the TP levels in the body.[31,102] Among the various analytical techniques, electrochemical sensors stand out as the favorable choice, offering swift and cost-effective means for the real-time quantification of TP within a clinical context. Thus, this review presents a comprehensive exploration of the electrochemical sensors utilized for TP monitoring, with a particular emphasis on the use of carbon-based materials in the electrode system.

Electrochemical sensors for theophylline

Many studies have reported the fabrication of electrochemical sensors with various recognition elements such as physical (nanomaterials), chemical (functional groups), and biological (enzymes/nucleic acids) elements. Alternatively, electrochemical sensors that do not incorporate a biorecognition element offer notable advantages, including simplicity, cost-effectiveness, and stability.[103,104] Additionally, these sensors often exhibit high stability and reproducibility given that they do not rely on biological components, which can degrade over time or require specific environmental conditions.[105] This makes them suitable for a range of applications, where cost and durability are critical factors. However, the absence of a biorecognition element also presents significant disadvantages. The selectivity of these sensors is generally lower compared to that incorporating biorecognition elements, which provides high specificity for the target analyte and significantly reduces the interference from other substances present in the samples.[106] Thus, although electrochemical sensors are advantageous due to their simplicity, low cost, and stability, careful consideration of the application design is crucial to address their selectivity and sensitivity limitations.

In recent decades, electrochemical sensors have become one of the most popular TP detection methods. The development of nanomaterial-modified electrochemical sensors can provide many advantages over the use of bare electrodes, such as wide surface area, excellent electrocatalytic activity, oxidation resistance, and fast electron transfer. In this case, the use of carbon-based nanomaterials as an electrode-modifying element is advantageous because their structure is easy to combine with various other functional materials.[12] The authors explained the effect of modifying several CNM, such as graphene, CNT, ND, and other carbons for improving the performance of sensors.

Graphene

Graphene-based nanomaterials possess a wide specific surface area, electronic conductivity, mechanical resistance, excellent

stability and biocompatibility, excellent binding capacity with biomolecules, and low toxicity.[31,102] Graphene is one of the nanocarbons that is very promising for combining with various materials. The surface of graphene contains abundant functional groups, which support the binding of functional materials.[107] To date, graphene-based TP sensors have not been widely explored, but the development of graphene-based electrodes is very promising.

Shetti *et al.* combined graphene oxide (GO) nanoparticles and nanoclay (NC) to increase the sensitivity and selectivity of a sensor and increase its biocompatibility as a material modifier for CPE.[31] NC is a material produced from the chemical weathering of various silicate minerals, which contains 85% of layered silicate minerals or layered chain silicate minerals of the total crustal mass.[108] NCs possess a porous structure, wide specific surface area, and high absorption efficiency and ionic conductivity.[109] NC-GO composites provide a wide surface area ratio and significant strengthening potential. In TP measurements, the peak current experienced a significant increase at pH 5, which was due to the increased electrocatalytic effect. Increasing the scan rate indicated a potential shift in the positive direction and an increase in peak current. This indicated that the measurements were controlled by an adsorption process with the involvement of single electrons and protons. The prepared sensor could detect TP in pharmaceutical samples with a reliable recovery rate of up to 98% and a detection limit as low as 0.001 μM.

Alternatively, Killedar *et al.* modified a GCE with GO and NC composites using the drop-casting method.[110] The study of the electrochemical behavior of TP showed a significant TP oxidation peak current in the GO-NC-modified GCE. In a previous study, the highest TP peak current was achieved at pH 5,[31] and the TP detection process occurred through an oxidation reaction involving the loss of 2 electrons. This reaction mechanism occurred on the electrode surface through a diffusion process, and the plausible reaction mechanism is shown in Fig. 2. The sensor showed acceptable selectivity towards TP in the presence of excipients and interfering ions. In addition, this sensor could detect TP in a wide concentration range of 0.1 to 20 μM. The detection of TP in tablet samples showed a recovery rate of up to 97%.

Shanbhag *et al.* fabricated a CPE-based sensor-modified GO interspersed with cholesterol (CHL-GO/CPE).[111] This sensor had hydrophilic and polar hydroxyl groups, which promoted the non-covalent hydrophobic π–π interactions with the GO sheets, thereby increasing the roughness and adsorption capacity for the analytes. In addition, CHL facilitated the transport of molecules across the membrane, and also increased the surface area.[112] Voltammetric measurements showed rapid electron transfer and an increase in the peak current for TP oxidation. This occurred significantly at pH 6 in an irreversible manner involving 2 protons and 2 electrons controlled by adsorption. The prepared sensor had high sensitivity and selectivity, with a low detection limit, reaching 0.004 μM and a recovery percentage in drug samples of nearly 99%. In another report, Kesavan *et al.* modified graphene onto the surface of a GCE with a melamine diazotization protocol to produce a stable graphene layer with a controllable thickness.[102] The graphene-modified GCE sensor could selectively detect TP in the presence of up to 34-fold excess adenosine. TP determination could be carried out stably even after 5 measurement cycles, with a low LOD value of 0.005 μM and reliable recovery in human urine and serum samples up to 99%.

Patil *et al.* fabricated a CPE-based TP sensor modified by a composite of GO and CuO NPs (CuO-GO/CPE).[113] The combination of GO and CuO NPs could accelerate electron transfer reactions at lower potentials and increase the capacitance of each material. GO supported by CuO NPs produced electrocatalysis and excellent power density.[114] The CuO-GO composite-modified CPE was fabricated by mixing graphite powder, paraffin oil, GO, and CuO NPs, with a ratio of GO and CuO NPs of 1 : 1, and the electrochemical behavior of TP was investigated in pH 6 PBS. The voltammetric measurements showed that the modified sensor had superior sensitivity and better selectivity. The interference test showed that there was no interference between several excipients and metal ions, including ascorbic acid, urea, lactose, NaCl, and KCl, at the oxidation peak of TP. The prepared electrode could detect TP with a low detection limit of 0.008 μM and an excellent recovery rate in human urine and serum samples of 98%.

Chen *et al.* modified a GCE with GO sheet nanocomposites decorated with rutile-type TiO_2 microspheres to form TiO_2 MPs@GOS/GCE.[115] TiO_2 is photochemically stable but has a wide band gap, and thus it was composited with GO to narrow its band gap or produce a new donor energy vacancy level.[116] The electrocatalytic properties of TiO_2 significantly improved the electrochemical behavior of TP. The fabrication of this electrode was quite simple and benefited from the regeneration of the electrode surface. The prepared sensor showed high selectivity and did not cause significant reactions to interfering molecules. Additionally, this sensor had a very wide linear concentration range of 0.02 to 209.6 μM and a detection limit as low as 0.013 μM. The successful application of this electrode for the determination of TP in drug samples and biological fluids was proven by its reliable recovery range of 96–103%.

Ghanbari *et al.* developed a sensitive and selective TP sensor based on a multinary nanocomposite-modified GCE consisting of core–shell TiO_2@CuO nanoparticles, boron-doped RGO, Au nanoparticles, and electropolymerized 2-amino-5-mercapto-1,3,4-thiadiazole (PAMT/AuNPs/TiO_2@CuO-B/RGO/GCE), as shown in Fig. 3.[117] Doping graphene with boron (B/RGO) aims to add electrons to its π-bonding system, increase its carrier density, and increase its electron transport rate.[118,119] B/RGO was

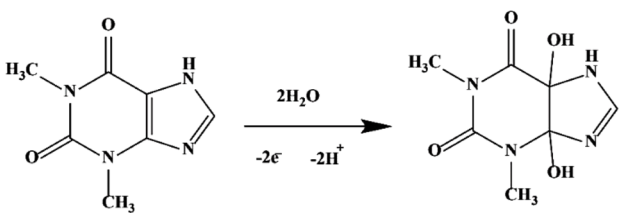

Fig. 2 Plausible reaction mechanism of TP. Reprinted with permission from ref. 110, Copyright (2021), Elsevier.

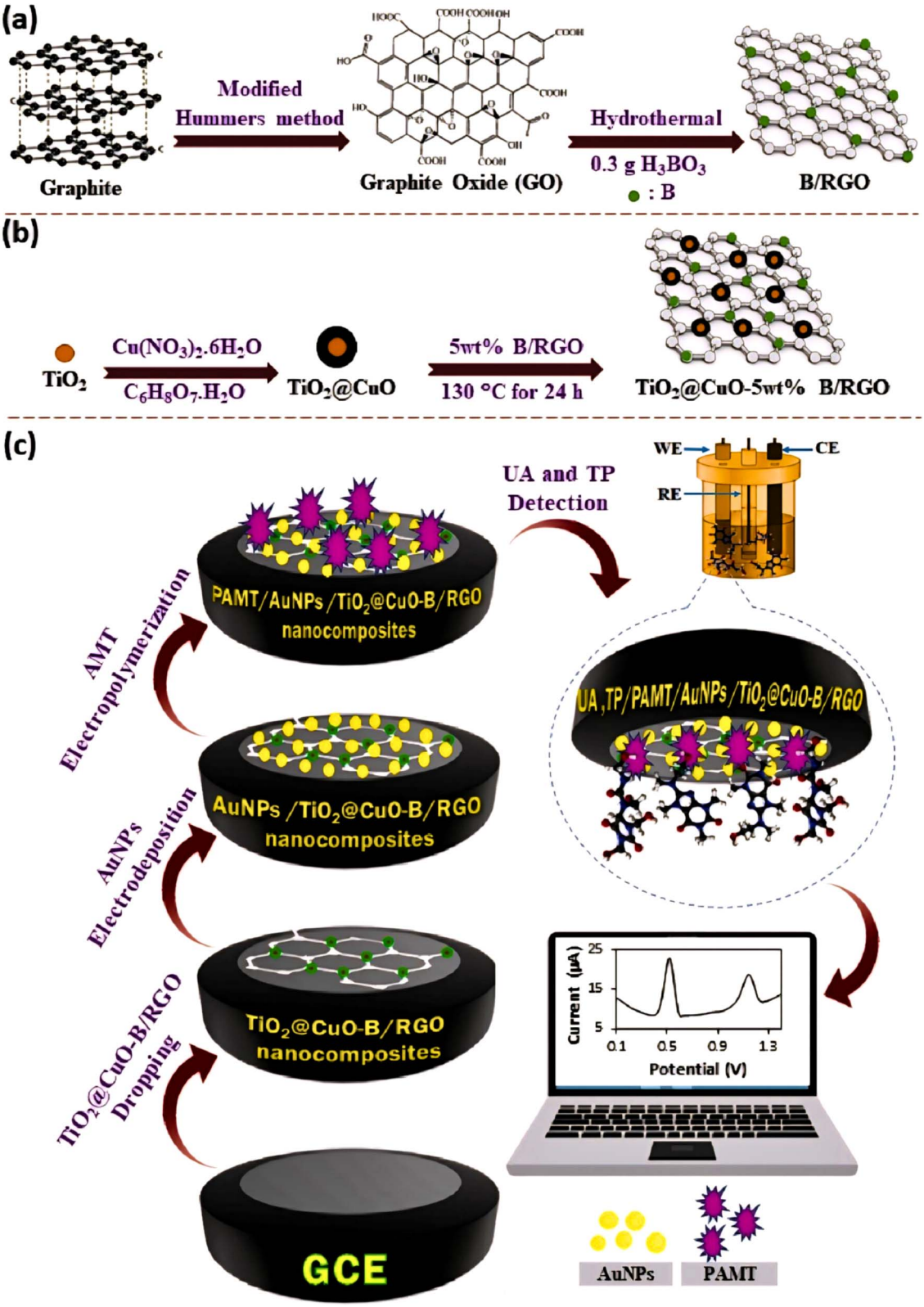

Fig. 3 Procedure for the preparation of (a) B/RGO nano-sheet, (b) TiO_2@CuO-B/RGO nanocomposites, and (c) design of electrochemical sensor for the simultaneous detection of UA and TP by the PAMT/AuNPs/TiO_2@CuO-B/RGO nanocomposite. Reprinted with permission from ref. 117. Copyright (2023), Elsevier.

combined with TiO_2@CuO core–shell nanoparticles and Au NPs to provide fast and excellent electron transfer kinetics between the electrode surface and the adsorbed bio-molecules *via* electrostatic interactions.[120] Electropolymerization of 5-amino-2-mercapto-1,3,4-thiadiazole into PAMT was carried out to increase the activity, stability, and biocompatibility of the sensor.[121] This sensor could detect TP in a wide linear concentration range of 0.001–10 μM with a very low detection limit of 0.0003 μM. This sensor also exhibited a reliable TP recovery rate of up to 103% in blood serum samples.

Hamidi and Zarei modified a GCE with an RGO-SDS-Nafion composite film.[122] Modification of the GCE with SDS and Nafion aimed to increase the rate of electron transfer between the analyte and the electrode surface, as well as providing high permeability properties to the cations originating from Nafion.[123,124] The RGO-SDS-Nafion/GCE sensor detected TP based on the preconcentration of positively charged TP molecules on the negatively charged SDS-Nafion in the composite film.[122] The optimal TP determination was achieved at acidic pH due to the more effective adsorption and accumulation of $1 \cdot H^+$ on the electrode surface due to ion exchange and electrostatic attraction by SDS and Nafion.[125] Additionally, it was found that most species, of the more than 20 interfering species used, did not interfere with the determination of TP, and thus it can be considered that this sensor had remarkable selectivity. Furthermore, this sensor had a low detection limit, as low as 0.005 μM, and could be used for TP determination in tablet samples with a satisfactory recovery rate of up to 104%.

Zhang *et al.* fabricated a TP sensor based on a GCE-modified poly(L-phenylalanine)/RGO composite film.[126] In this work, RGO was prepared by the electrochemical reduction method because it resulted in higher conductivity and lower oxygen/carbon ratio than the chemical reduction method.[127,128] Polymer modification of the electrode was performed to improve electrocatalysis, while reducing surface fouling and undesirable reactions.[129,130] The P(L-pal)/RGO composite film was electropolymerized on the GCE using the CV technique. This sensor could be used to determine TP and caffeine simultaneously, and also be used in the long term and showed reliable reproducibility and selectivity. The prepared electrode could detect TP and caffeine in real samples with the recovery percentage reaching 102%.

As shown in Fig. 4a, TP sensing using the same electrochemical technique could produce different peak currents and potentials at different electrode and modifiers. This showed that the type of electrode and type of modifying material affect the sensitivity, selectivity, precision, and accuracy of the sensor.

Carbon nanotubes

CNTs are CNMs that are the most suitable for functionalization with any material. As modifier elements, CNTs can facilitate wide surface areas and rich binding active sites, thereby enabling sensors to detect a wide range of analytes. Currently, the development of CNT-modified electrochemical sensors has not been widely carried out, and thus still very prospective.

In the study by da Silva *et al.*, MWCNTs decorated with AuNPs were deposited on a GCE (AuNP-MWCNT/GCE) to develop a new conductive platform for the determination of TP.[132] The modification of AuNPs on MWCNTs was carried out by the direct dispersion of AuNPs into the MWCNT network. The unique electronic properties of AuNPs can provide various advantages when combined with tube-structured nanocarbons.[133,134] There was an increase in the peak current of TP oxidation, which was attributed to the effective surface area and the synergistic effect of AuNP aggregation on the MWCNT net.[135] The sensor could be made quickly and easily, and its architecture was not very complicated. Furthermore, it could detect TP at low concentrations, down to 0.09 μM, and showed a recovery percentage of approximately 97–110% in commercial samples, exhibiting potential for application in therapeutic drug monitoring and tea quality control.

Iranmanesh *et al.* synthesized La_2O_3/MWCNT nanocomposites as sensing elements for the determination of TP.[136] They exhibited a respectable dielectric constant, low oxide

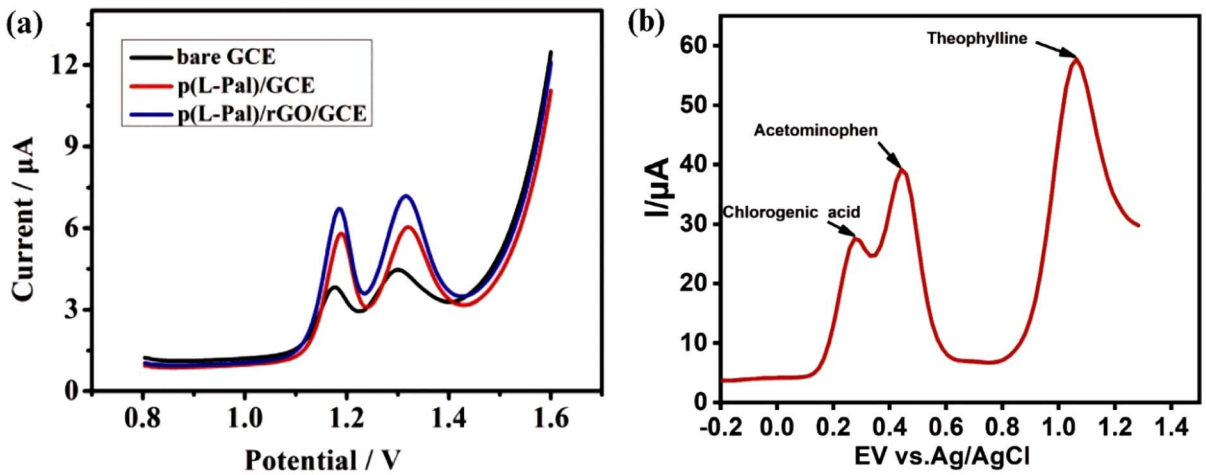

Fig. 4 (a) DPV of 40 μM TP on different electrodes in 10 mM H_2SO_4. Reprinted with permission from ref. 126. Copyright (2021), Elsevier and (b) DPV of 0.1 M TP current response on ZnONPs-MWCNTs-Cyt c-GCE electrode with the addition of various interfering species. Reprinted with permission from ref. 131. Copyright (2020), Elsevier.

leakage current, and an increased voltage range, making them alternative materials for the fabrication of environmentally friendly sensors for various analytes.[137,138] TP detection was carried out on the GCE-modified La_2O_3/MWCNTs (La_2O_3/MWCNTs/GCE). Under the optimal conditions, this sensor could be used to detect TP over a wide concentration ranging from 0.1 to 400 μM. Furthermore, it exhibited high sensitivity with a low detection limit as low as 0.032 μM and an excellent TP recovery rate in blood serum and urine samples up to 100%.

Koçak *et al.* synthesized a composite of CNT and symmetrically substituted manganese(III) phthalocyanine (2eOHMnPc) containing a tetra-5-chloroquinolin-8-yloxy group at the peripheral position (2eOHMnPc-CNT).[139] The combination of CNTs and 2eOHMnPc could increase the stability and increase the conductivity of both materials in electrochemical applications. In this study, 2eOHMnPc-CNT was modified on the surface of GCE and the prepared electrode had excellent stability and could be used in the long term without any apparent loss of more than 9.0%. In addition, the sensitivity and selectivity of the sensor were also improved by the presence of the 2eOHMnPc-CNT composite. Also, the individual detection of TP was successfully achieved in green tea and serum TP samples.

Rezvani *et al.* developed a TP electrochemical sensor based on a WO_3/MWCNT nanocomposite modified GCE (WO_3/MWCNT/GCE).[140] WO_3 nanoparticles are n-type semiconductors that have unique electrochemical redox characteristics.[141,142] Alternatively, WO_3 has low electronic conductivity, but when combined with MWCNTs, its conductivity could be increased and the capacitive behavior of the composite can also be impressively improved.[143] The large electroactive area and conductivity of the nanocomposite made the sensor more sensitive and it could detect TP at low concentrations, reaching 0.008 μM, and it increased the selectivity of the sensor in the presence of various interfering molecules. Furthermore, it could be used for TP determination in real samples without any previous separation steps.

Kilele *et al.* modified GCE with a ZnONP-MWCNT-Cyt c nanocomposite.[131] ZnONPs are semiconductor materials that have an excitation binding energy of 60 meV and superior electrocatalytic properties.[144,145] ZnONPs were combined with MWCNTs to increase the electron transfer rate and adsorption ability. In this study, the cytochrome c enzyme was immobilized on the ZnONP-MWCNT nanocomposites to increase the specificity of the sensor for TP determination.[146,147] The prepared biosensor exhibited high selectivity and could be used to detect TP in pharmaceutical syrup without significant interference by the presence of interfering substances, as shown in Fig. 4b. TP determination could be carried out at low concentrations of up to 0.0012 μM. In addition, this biosensor could be used for long-term measurements and has potential to be used in the qualitative and quantitative analysis of drugs and other electroactive target compounds.

Studies on the application of CNTs as electrode or modifier materials have not yet been widely reported. However, several of the studies discussed previously indicated that CNTs have promising opportunities in electrochemical sensor applications. Moreover, their structure is rich in binding sites, making them advantageous in the manufacture of nanocomposites and structure modification.

Nanodiamonds

NDs represent a 3D carbon allotrope, typically ranging in size from 5 to 50 nm, which are often used for biomedical and pharmaceutical purposes due to their negligible toxicity, inert core, rich surface chemistry, and bright and strong fluorescence properties.[148] ND-based electrochemical sensors are rarely reported,[149] including TP sensors, and thus study opportunities for novel systems based on NDs are wide open.

Diamonds that were doped with boron (BDD) provided increased electrical conductivity and have the potential to become better electrodes than pure NDs.[150] BDD exhibits unique electrochemical properties, such as excellent chemical and dimensional stability, low background current, and wide potential window.[151] Another advantage of BDD-based electrochemical electrodes is the stability of their response and material durability, which does not require pretreatment or maintenance of the electrode.[152]

The BDD electrochemical oxidation of TP was first demonstrated, and using different voltammetric methods, a TP electrochemical sensor with a BDD electrode was reported using DPV and SWV.[153] As shown in Fig. 5a, the irreversible peak for the direct oxidation of the analyte was observed with CV and formed at +1.63 V (*vs.* Ag/AGCEl electrode) in 1 M H_2SO_4. The results of this study indicated the possibility of reducing the matrix effect by employing aqueous solutions at a large anodic potential.

Modification of a BDD electrode with nickel nanoparticles (BDD/NiNP) using the electrodeposition method was successfully carried out for the TP electrochemical sensor.[154] As shown in Fig. 5b, the peak of TP appeared in CV in the potential range of +1.20 to +1.50 V (*vs.* Ag/AgCl). Based on the CV analysis, the active surface area of the BDD/NiNP electrode was 0.0081 cm^2, which was greater than that of the unmodified BDD area of 0.0011 cm^2, and selective for D-glucose, ammonium sulfate, and urea.

Other carbon nanomaterials

Electrochemical sensors based on a modified glassy carbon (GCE) and carbon paste electrode are the most frequently reported among the carbon materials, which were summarized compared in a table previously.[157] The recent report was the novel detection of TP with GCE-modified carbon dots (CDs) and chitosan (Chi).[155] The electrochemical characteristics of the electrode were evaluated with CV in 0.01 M $K_3[Fe(CN)_6]$, as shown in Fig. 5c, showing more efficient electron transfer. The quasi-reversible process was characterized by the anodic peak current/cathodic peak current ratio (I_{ap}/I_{cp}), which was between 0.81 and 1.33, and the difference between the anodic peak potential and cathodic peak potential (ΔE_p) ranged from 0.22 to 0.08 V. The selectivity of the sensor was tested with ferulic acid, 5-caffeoylquinic acid, catechin, and epicatechin interference solution.

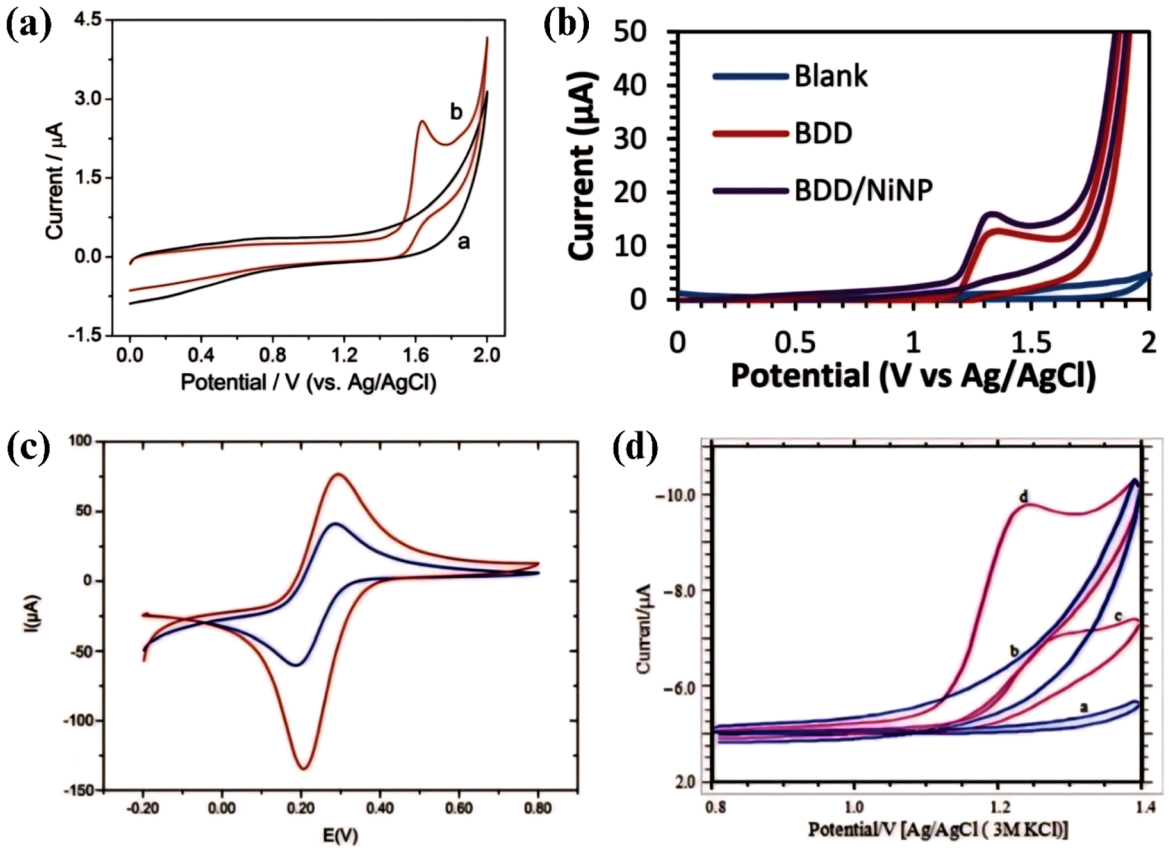

Fig. 5 (a) CV of blank (a) and TP (b) in H_2SO_4 on the BDD electrode. Reprinted with permission from ref. 153, Copyright (2015), The Royal Society of Chemistry. (b) CV of the blank (0.1 M PBS) for the BDD electrode (blue), BDD (red) and BDD/NiNP electrode (purple) in 60 μM TP,[154] (c) CV of bare recorded at GCE (blue) and GCE/Chi-CDs (red),[155] and (d) CV of CPE on PBS pH 3.0 (a), CPE/MB on PBS pH 3.0 (b), CPE on PBS containing TP (c), and CPE/MB on PBS containing TP (d). Reprinted with permission from ref. 156 Copyright (2018), Elsevier.

Another study reported the modification of a GCE with CDs produced by one-step ultrasonic technology with a glucose precursor *via* electrochemical deposition for the detection of TP.[158] CDs were evenly distributed on the GCE. This electrode could amplify the weak and partially overlapping peaks of dopamine, uric acid, L-tryptophan, and TP. Dopamine, uric acid, L-tryptophan, and TP were significantly observed by 4 well-identified oxidation peaks despite the presence of coexisting interferences in biological fluids due to the superior electrode biocompatibility.

In the realm of CNM, multilayer fullerene represents one of the latest fullerene families, also referred to as carbon nano-onions (CNOs).[159] It has high thermal stability and high electrical conductivity and has attracted attention for the development of sensors.[160] CNOs with a size of 5–10 nm were prepared by the stepwise multipotential method and deposited on a GCE by the drop-coating method for the fabrication of a TP detection sensor.[161] GCE/CNOs promoted the sensitivity of the sensor, exhibiting a detection limit as low as 0.35 μM, reliable repeatability, and excellent anti-interference ability.

The acceptable catalytic properties and biocompatibility of sulfosalicylic acid polymers were used to fabricate novel carbon nanofibers (CNFs) as a stable sensor for the detection of TP in drug analysis.[162] CNFs are novel CNM with similar conductivity and stability as CNTs.[163] The electrospun carbon fibers were strong and flexible enough for use as sensor or electrode materials.[164] Under the optimal experimental conditions, the TP concentration (0.6–137 M) and peak current value showed an acceptable linear range and the detection limit was as low as 0.2 M.

The carbon paste electrode (CPE) is known as an easy-to-fabricate electrode with easily chemically modified surfaces for the analysis of inorganic and organic species.[165] Details and practical guidance for experimental laboratory work, with several practical hints and recommendations on various types of chemically and biologically modified CPEs were previously reported for electroanalysis purposes.[166] In TP electrochemical sensors, several CPE modifications have been applied. For example, CPE, which is graphite powder mixed with MWCNT-functionalized CuO nanoparticles and ionophores, showed a relatively stable sensor for 46 days with an LOD of 2.5×10^{-8} M and was tested for the detection of TP in various green tea extracts, which had undergone filtration, dilution, and pH modification.[167] Other modifications for detecting TP in food are CPE modified with nano-sized cobalt (nano-CoPc),[168] metal phthalocyanine (MPc) derivatives known as electrocatalysts to catalyze the oxidation or reduction of several species, and CPE-modified single-walled carbon nanotube composites decorated

with Fe_3O_4 and 1-ethyl-3-methyl imidazolium chloride (CPE/1E3MICl/Fe_3O_4/SWCNTs) composite.[169] CPE/nano-CoPc showed excellent reproducibility and stability compared with bulk CoPc complexes, while CPE/1E3MICl/Fe_3O_4/SWCNTs showed a strong ability to resolve overlapping xanthine (XT) and TP signals of ~280 mV.

In a detection system on human plasma, CPE was modified with graphene and ethyl 2-(4-ferrocenyl-[1,2,3]triazol-1-yl) acetate (CPE-EFTAG)[170] and MWCNTs.[171] CPE-EFTAG could determine isoproterenol, acetaminophen, tryptophan, and TP simultaneously in real plasma samples with significant differences, namely 0.190 V between isoproterenol and acetaminophen, 0.510 V between isoproterenol and tryptophan, and 0.750 V between isoproterenol and TP. Meanwhile, CPE/MWCNT could determine linezolid, meropenem, and TP in spiked plasma and healthy volunteer plasma.

Table 1 Carbon-based materials for the electrochemical detection of theophylline

Electrode	Detection method	LOD (μM)	Linear range (μM)	Electrolyte	pH	Sample	Recovery (%)	Ref.
GO-NC/CPE	CV, SWV	0.0018	0.01–0.2	PBS	5.0	Pharmaceutical formulations	96.9–98.31	31
GO-NC/GCE	SWV	0.00312	0.1–2.0	PBS	5.0	Pharmaceutical tablet	94.7–97.4	110
CHL-GO/CPE	CV, LSV, SWV	0.00445	0.1–3.0	PBS	6.0	Tablet	96.5–98.8	111
G/GCE	CV, DPV	0.0054	0.03–100.0	PBS	6.0	Human serum	98.6–99.2	102
						Urine	99.0–99.3	
CuO-GO/CPE	CV, DPV	0.00833	0.1–3.5	PBS	6.0	Urine	95.0–98.75	113
						Tablet	98.0	
TiO_2 MPs@GOS/GCE	CV, DPV	0.01326	0.02–209.6	PBS	7.0	Human serum	96.8–103.0	115
						Drug	96.3–98.6	
PAMT/AuNPs/TiO_2@CuO-B/RGO/GCE	CV, DPV	0.00036	0.001–10.0	PBS	6.0	Blood serum	94.0–103.0	117
RGO-SDS-Nafion/GCE	CV, DPV	0.005	0.01–40.0	H_2SO_4	—	Tablet	97.5–104.5	122
P(L-Pal)/rGO/GCE	CV, DPV	0.35	1.0–260.0	H_2SO_4	1.7	Tablet	102.0	126
AuNP-MWCNT$_{0.25}$/GCE	DPV	0.09	0.5–20	BR buffer	6.0	Tablets	98.0–110.0	132
						Black tea	97.3–105.3	
						Green tea	97.3–107.3	
La_2O_3/MWCNT/GCE	CV, DPV	0.032	0.1–400.0	PBS	7.0	Human blood serum	97.5–101.3	136
						Urine	98.6–102.0	
2eOHMnPc-CNT/GCE	CV, DPV	0.0066	0.04–12.0	H_2SO_4	2.0	Serum	102.0	139
						Green tea	97.8	
WO_3/MWCNT/GCE	AdsDPV	0.008	0.025–2.6	H_2SO_4	1.3	Tablet	98.5–101.8	140
						Urine	98.2–104.0	
ZnONPs-MWCNTs-Cyt c-GCE	CV, DPV	0.0012	0.4–15.0	PBS	3.5	Pharmaceutical formulations	99.4–106.8	131
BDD	DPV	0.91	2.0–380.0	H_2SO_4	1.47	Pharmaceutical tablets	98.0–103.3	153
	SVW	1.45				Human urine	93.2–102.2	
BDD	CV, SWV	4.58	30.0–100.0	PBS	3.0	Artificial urine	99.87	154
BDD/NiNP		2.79					105.10	
CDs-Chi/GCE	CV, DPV	1.0	10.0–5000.0	$HClO_4$	0.4	Tea, drug	30.0–50.0	155
CDs/GCE	CV, DPV	0.33	10.0–200.0	PBS	6.0	Human serum	98.79–101.9	158
CNOs/GCE	DPV	0.35	8.16–108.25	PBS	7.0	Human serum	96.03–99.96	161
CNF/PSA/GCE	CV, DPV	0.2	0.6–137.0	H_2SO_4–Na_2SO_4	1.8	Tablet	98.6–103.4	162
CuO/MWNCT/CPE	Potentiometric	0.025	0.1–10000.0	PBS	6.0	Commercial tea	92.00–99.63	167
Nano-CoPc/CPE	DPV	0.14	0.4–100.0	PBS	7.4	Pharmaceutical tablet	97.1–103.1	168
						Green tea	97.5–102.1	
SWCNT/Fe_3O_4/1E$_3$MICl/CPE	SWV	—	0.1–300.0	PBS	6.0	Fruit juice drink	101.4–104.8	169
						Fish meat	102.5	
EFTAG/CPE	CV, SWV	15.0	20.0–1000.0	PBS	7.0	Human blood serum	98.6–103.7	170
						Urine	99.6–103.7	
MWCNT/CPE	SWV	0.194	0.8–90.0	BR Buffer	3.0	Human plasma	83.17–89.29	171
MB/CPE	CV, DPV	0.00225	0.2–10.0	PBS	3.0	Pharmaceutical tablet	99.2–100.3	156
						Urine	98.6–100.4	

Another report on the electrochemical oxidation of TP was found on the surface of CPE with the cationic dye methylene blue (MB) as an excellent electron mediator.[156] MB could be quickly degraded by electrochemical oxidation with excellent performance in the pH range of 3.0–11.0 and consumed the electrical energy of 21.35 kW h m^{-3}, which is lower than that of electro-Fenton (81.51 kW h m^{-3}) and electro-coagulation (36.55 kW h m^{-3}).[172] The single electrochemical oxidation of TP was dominant at pH 3.0 and CV scan speed of 50 mV s^{-1} (Fig. 5d) and was successfully used for the determination of TP in pharmaceutical samples and human urine. The peak current of CPE/MB increased sharply by 2–3 times compared to bare CPE where electron transfer occurred slowly and sluggishly. The increase in peak current was entirely due to the presence of MB given that it was an excellent redox mediator and provided easy electron transfer.

The key points of the overall other carbon electrochemical TP sensors are presented in Table 1 for ease of comparison. The potential for the development of electrochemical sensors to detect TP, whether through modifications to existing electrodes or the introduction of new sensor technologies, is wide open.

Conclusions

In conclusion, this review meticulously outlined the recent advancements in the use of carbon-based electrodes, including NDs, graphene derivatives, and CNTs, in the electroanalytical method for the detection of TP. These materials significantly enhanced the sensitivity, LOD, selectivity, and real sample applications. Continued innovation in carbon-based electrode materials holds promise for improving the capabilities of electrochemical sensors for the detection of TP. Future reports can focus on refining the fabrication techniques, exploring new carbon-based composites, and integrating advanced technologies for greater precision. The ongoing evolution of carbon-based materials not only supports pharmaceuticals but also holds potential for broader applications in biosensing and clinical diagnostics, promising a bright future for TP sensors and electrochemical approaches.

Data availability

No primary research results, software or code have been included and no new data were generated or analysed as part of this review.

Conflicts of interest

There were no conflicts to declare.

Acknowledgements

The authors acknowledged the funding from Universitas Airlangga by International Report Consortium (IRCON) study scheme with grant number 191/UN3.LPPM/PT.01.03/2024.

References

1 M. Cazzola, C. P. Page, L. Calzetta and M. G. Matera, *Pharmacol. Rev.*, 2012, **64**, 450–504.
2 P. J. Barnes, *Am. J. Respir. Crit. Care Med.*, 2013, **188**, 901–906.
3 N. Katiyar, L. S. Selvakumar, S. Patra and M. S. Thakur, *Anal. Methods*, 2013, **5**, 653–659.
4 P. Chen, J. Shen, C. Wang and Y. Wei, *Microchim. Acta*, 2018, **185**, 113.
5 M. S. Bispo, M. C. C. Veloso, H. L. C. Pinheiro, R. F. S. De Oliveira, J. O. N. Reis and J. B. D. Andrade, *J. Chromatogr. Sci.*, 2002, **40**, 45–48.
6 S. K. Hassaninejad-Darzi, A. Samadi-Maybodi and S. M. Nikou, *Iran. J. Pharm. Res.*, 2016, **15**, 379–391.
7 T. Tunali Akbay, H. Ipekci and A. Yarat, *J. Anal. Chem.*, 2020, **75**, 640–644.
8 X. Ma, Z. Guo, Z. Mao, Y. Tang and P. Miao, *Microchim. Acta*, 2018, **185**, 33.
9 P. K. Jiwanti, I. R. Sitorus, G. T. M. Kadja, S. Wafiroh and Y. Einaga, *Indones. J. Chem.*, 2022, **22**, 1321–1329.
10 T. A. Ivandini, J. Ariani, P. K. Jiwanti, J. Gunlazuardi, E. Saepudin and Y. Einaga, *Makara J. Sci.*, 2017, **21**, 34–42.
11 T. Matsunaga, T. Kondo, I. Shitanda, Y. Hoshi, M. Itagaki, T. Tojo and M. Yuasa, *Carbon*, 2021, **173**, 395–402.
12 P. K. Jiwanti, B. Y. Wardhana, L. G. Sutanto and M. F. Chanif, *ChemistrySelect*, 2022, **7**, e202103997.
13 B. Uslu and S. A. Ozkan, *Anal. Lett.*, 2007, **40**, 817–853.
14 Y. Li, S. Wu, P. Luo, J. Liu, G. Song, K. Zhang and B. Ye, *Anal. Sci.*, 2012, **28**, 497–502.
15 S. MansouriMajd, H. Teymourian, A. Salimi and R. Hallaj, *Electrochim. Acta*, 2013, **108**, 707–716.
16 S. Yang, R. Yang, G. Li, J. Li and L. Qu, *J. Chem. Sci.*, 2010, **122**, 919–926.
17 K. P. Gopinath, D. V. N. Vo, D. Gnana Prakash, A. Adithya Joseph, S. Viswanathan and J. Arun, *Environ. Chem. Lett.*, 2021, **19**, 557–582.
18 M. Azizi-Lalabadi, H. Hashemi, J. Feng and S. M. Jafari, *Adv. Colloid Interface Sci.*, 2020, **284**, 102250.
19 Y. Pan, X. Liu, W. Zhang, Z. Liu, G. Zeng, B. Shao, Q. Liang, Q. He, X. Yuan, D. Huang and M. Chen, *Appl. Catal., B*, 2020, **265**, 118579.
20 Z. Peng, X. Liu, W. Zhang, Z. Zeng, Z. Liu, C. Zhang, Y. Liu, B. Shao, Q. Liang, W. Tang and X. Yuan, *Environ. Int.*, 2020, **134**, 105298.
21 A. O. Egbedina, O. P. Bolade, U. Ewuzie and E. C. Lima, *J. Environ. Chem. Eng.*, 2022, **10**, 107260.
22 N. P. Shetti, S. J. Malode, D. S. Nayak, G. B. Bagihalli, K. R. Reddy, K. Ravindranadh and C. V. Reddy, *Microchem. J.*, 2019, **149**, 103985.
23 Z. Liu, K. Nørgaard, M. H. Overgaard, M. Ceccato, D. M. A. Mackenzie, N. Stenger, S. L. S. Stipp and T. Hassenkam, *Carbon*, 2018, **127**, 141–148.
24 M. M. Sabzehmeidani, S. Mahnaee, M. Ghaedi, H. Heidari and V. A. L. Roy, *Adv. Mater.*, 2021, **2**, 598–627.

25 S. Priyadarsini, S. Mohanty, S. Mukherjee, S. Basu and M. Mishra, *J. Nanostruct. Chem.*, 2018, **8**, 123–137.
26 A. T. Smith, A. M. LaChance, S. Zeng, B. Liu and L. Sun, *Nano Mater. Sci.*, 2019, **1**, 31–47.
27 K. Ling, H. Jiang, Y. Li, X. Tao, C. Qiu and F. R. Li, *Biosens. Bioelectron.*, 2016, **86**, 8–13.
28 R. Petrucci, I. Chiarotto, L. Mattiello, D. Passeri, M. Rossi, G. Zollo and M. Feroci, *Molecules*, 2019, **24**, 4247.
29 S. Priyadarsini, S. Mohanty, S. Mukherjee, S. Basu and M. Mishra, *J. Nanostruct. Chem.*, 2018, **8**, 123–137.
30 V. N. Nguyen, D. T. Tran, M. T. Nguyen, T. T. T. Le, M. N. Ha, M. V. Nguyen and T. D. Pham, *Res. Chem. Intermed.*, 2018, **44**, 3081–3095.
31 N. P. Shetti, S. J. Malode, D. S. Nayak, G. B. Bagihalli, K. R. Reddy, K. Ravindranadh and C. V. Reddy, *Microchem. J.*, 2019, **149**, 103985.
32 J. Li, D. Kuang, Y. Feng, F. Zhang, Z. Xu, M. Liu and D. Wang, *Biosens. Bioelectron.*, 2013, **42**, 198–206.
33 M. Azizi-Lalabadi, H. Hashemi, J. Feng and S. M. Jafari, *Adv. Colloid Interface Sci.*, 2020, **284**, 102250.
34 S. K. Tiwari, S. Sahoo, N. Wang and A. Huczko, *J. Sci.: Adv. Mater. Devices*, 2020, **5**, 10–29.
35 A. T. Smith, A. M. LaChance, S. Zeng, B. Liu and L. Sun, *Nano Mater. Sci.*, 2019, **1**, 31–47.
36 S. J. Rowley-Neale, E. P. Randviir, A. S. Abo Dena and C. E. Banks, *Appl. Mater. Today*, 2018, **10**, 218–226.
37 M. T. U. Malik, A. Sarker, S. M. S. Mahmud Rahat and S. B. Shuchi, *Mater. Today Commun.*, 2021, **28**, 102685.
38 W. Zheng, M. Zhao, W. Liu, S. Yu, L. Niu, G. Li, H. Li and W. Liu, *J. Electroanal. Chem.*, 2018, **813**, 75–82.
39 K. Atacan, *J. Alloys Compd.*, 2019, **791**, 391–401.
40 P. Tian, L. Tang, K. S. Teng and S. P. Lau, *Mater. Today Chem.*, 2018, **10**, 221–258.
41 M. Li, T. Chen, J. J. Gooding and J. Liu, *ACS Sens.*, 2019, **4**, 1732–1748.
42 M. M. A. Aslam, H. W. Kuo, W. Den, M. Usman, M. Sultan and H. Ashraf, *Sustainability*, 2021, **13**, 5717.
43 T. Shi, Z. Li, J. Guo, H. Gong and C. Gu, *Constr. Build. Mater.*, 2019, **202**, 290–307.
44 L. S. Salah, N. Ouslimani, D. Bousba, I. Huynen, Y. Danleé and H. Aksas, *J. Nanomater.*, 2021, **2021**, 4972770.
45 N. M. Nurazzi, F. A. Sabaruddin, M. M. Harussani, S. H. Kamarudin, M. Rayung, M. R. M. Asyraf, H. A. Aisyah, M. N. F. Norrrahim, R. A. Ilyas, N. Abdullah, E. S. Zainudin, S. M. Sapuan and A. Khalina, *Nanomaterials*, 2021, **11**, 2186.
46 S. K. Soni, B. Thomas and V. R. Kar, *Mater. Today Commun.*, 2020, **25**, 101546.
47 Y. Yi, B. Wang, X. Liu and C. Li, *Carbon Lett.*, 2022, **32**, 713–726.
48 M. Chen, Q. S. Jing, H. Bin Sun, J. Q. Xu, Z. Y. Yuan, J. T. Ren, A. X. Ding, Z. Y. Huang and M. Y. Dong, *Langmuir*, 2019, **35**, 6321–6332.
49 M. Chen, G. C. Wang, W. Q. Yang, Z. Y. Yuan, X. Qian, J. Q. Xu, Z. Y. Huang and A. X. Ding, *ACS Appl. Mater. Interfaces*, 2019, **11**, 42156–42171.
50 M. S. Yahya and M. Ismail, *J. Phys. Chem. C*, 2018, **122**, 11222–11233.
51 N. Janudin, N. Abdullah, W. M. Z. Wan Yunus, F. M. Yasin, M. H. Yaacob, N. Mohamad Saidi and N. A. M. Kasim, *J. Nanotechnol.*, 2018, **2018**, 2107898.
52 M. N. Norizan, M. H. Moklis, S. Z. Ngah Demon, N. A. Halim, A. Samsuri, I. S. Mohamad, V. F. Knight and N. Abdullah, *RSC Adv.*, 2020, **10**, 43704–43732.
53 Y. Zhang, K. Y. Rhee, D. Hui and S. J. Park, *Compos. B Eng.*, 2018, **143**, 19–27.
54 B. Sundqvist, *Phys. Rep.*, 2021, **909**, 1–73.
55 Y. Wu and T. Weil, *Adv. Sci.*, 2022, **9**, 2200059.
56 P. Karami, S. Salkhi Khasraghi, M. Hashemi, S. Rabiei and A. Shojaei, *Adv. Colloid Interface Sci.*, 2019, **269**, 122–151.
57 P. Karami, S. A. Aktij, B. Khorshidi, M. D. Firouzjaei, A. Asad, M. Elliott, A. Rahimpour, J. B. P. Soares and M. Sadrzadeh, *Desalination*, 2022, **522**, 115436.
58 D. Terada, T. Genjo, T. F. Segawa, R. Igarashi and M. Shirakawa, *Biochim. Biophys. Acta, Gen. Subj.*, 2020, **1864**, 129354.
59 Y. M. Hunge, A. A. Yadav, S. Khan, K. Takagi, N. Suzuki, K. Teshima, C. Terashima and A. Fujishima, *J. Colloid Interface Sci.*, 2021, **582**, 1058–1066.
60 M. Mehmandoust, P. Pourhakkak, F. Hasannia, Ö. Özalp, M. Soylak and N. Erk, *Food Chem. Toxicol.*, 2022, **164**, 113080.
61 R. Namdar and S. Nafisi, *Drug Discov. Today*, 2018, **23**, 1152–1158.
62 C. Lee, Y. Seo, J. Han, J. Hwang and I. Jeon, *Carbon*, 2023, **210**, 118041.
63 S. Yao, X. Yuan, L. Jiang, T. Xiong and J. Zhang, *Materials*, 2020, **13**, 2924.
64 P. Bhakta and B. Barthunia, *J. Indian Acad. Oral Med. Radiol.*, 2020, **32**, 159–163.
65 N. P. Shetti, A. Mishra, S. Basu and T. M. Aminabhavi, *Mater. Today Chem.*, 2021, **20**, 100454.
66 Y. Pan, X. Liu, W. Zhang, Z. Liu, G. Zeng, B. Shao, Q. Liang, Q. He, X. Yuan, D. Huang and M. Chen, *Appl. Catal., B*, 2020, **265**, 118579.
67 Y. Zhu, S. Huai, J. Jiao, Q. Xu, H. Wu and H. Zhang, *J. Electroanal. Chem.*, 2020, **878**, 114726.
68 Z. Peng, X. Liu, W. Zhang, Z. Zeng, Z. Liu, C. Zhang, Y. Liu, B. Shao, Q. Liang, W. Tang and X. Yuan, *Environ. Int.*, 2020, **134**, 105298.
69 V. N. Rao, N. L. Reddy, M. M. Kumari, K. K. Cheralathan, P. Ravi, M. Sathish, B. Neppolian, K. R. Reddy, N. P. Shetti, P. Prathap, T. M. Aminabhavi and M. V. Shankar, *J. Environ. Manage.*, 2019, **248**, 109246.
70 X. Wang, Y. Feng, P. Dong and J. Huang, *Front. Chem.*, 2019, **7**, 671.
71 Z. Hassanvand, F. Jalali, M. Nazari, F. Parnianchi and C. Santoro, *Chemelectrochem*, 2021, **8**, 15–35.
72 X. Li, L. Shi, L. Li, C. Dong, C. zhong Li and S. Shuang, *J. Anal. Test.*, 2019, **3**, 37–49.
73 S. Zhu, Y. Song, X. Zhao, J. Shao, J. Zhang and B. Yang, *Nano Res.*, 2015, **8**, 355–381.

74 H. A. M. Kerstjens, J. W. Upham and I. A. Yang, *J. Thorac. Dis.*, 2019, **11**, S2200–S2209.
75 Y. Shen, S. Huang, J. Kang, J. Lin, K. Lai, Y. Sun, W. Xiao, L. Yang, W. Yao, S. Cai, K. Huang and F. Wen, *Int. J. Chronic Obstruct. Pulm. Dis.*, 2018, **13**, 399–407.
76 N. Siafakas and A. Trachalaki, *Pulmonology*, 2023, **29**, S86–S91.
77 D. M. Williams and B. K. Rubin, *Respir. Care*, 2018, **63**, 641–654.
78 J. Perez-Garcia, E. Herrera-Luis, A. Li, A. C. Y. Mak, S. Huntsman, S. S. Oh, J. R. Elhawary, C. Eng, K. B. Beckman, D. Hu, F. Lorenzo-Diaz, M. A. Lenoir, J. Rodriguez-Santana, N. Zaitlen, J. Villar, L. N. Borrell, E. G. Burchard and M. Pino-Yanes, *J. Allergy Clin. Immunol.*, 2023, **151**, 1503–1512.
79 H. Madsen, D. P. Henriksen, V. Backer, H. C. Siersted, N. Bjerring and C. S. Ulrik, *J. Asthma*, 2021, **58**, 216–222.
80 A. W. M. Goorsenberg, J. N. S. d'Hooghe, K. Srikanthan, N. H. T. ten Hacken, E. J. M. Weersink, J. J. T. H. Roelofs, S. V. Kemp, E. H. Bel, P. L. Shah, J. T. Annema and P. I. Bonta, *Am. J. Respir. Crit. Care Med.*, 2021, **203**, 175–184.
81 D. Langton, A. Ing, K. Bennetts, W. Wang, C. Farah, M. Peters, V. Plummer and F. Thien, *BMC Pulm. Med.*, 2018, **18**, 155.
82 C. Henry, S. Biardel, M. Boucher, K. Godbout, J. Chakir, A. Côté, M. Laviolette and Y. Bossé, *Respir. Med.*, 2023, **217**, 107340.
83 J. Muddle, V. Kanabar, M. Brown, C. Page and B. Forbes, *Pulm. Pharmacol. Ther.*, 2020, **63**, 101943.
84 R. Miguel, C. Siddharth and V. Timothy, *J. Clin. Image Med. Case Rep.*, 2021, **2**, 1416.
85 C. A. Aliaga, L. F. de Arizon, R. M. Bermúdez, J. A. Ballarín Castán and A. V. Santandreu, *J. Nephrol.*, 2020, **42**, 250–253.
86 H. Funakoshi, K. Momo, K. Okazaki, T. Ebato, S. Yamamoto, T. Uno, S. Ohta, H. Sagara and T. Sasaki, *Br. J. Clin. Pharmacol.*, 2021, **87**, 3375–3377.
87 M. T. Wang, J. H. Lai, C. L. Tsai and J. T. Liou, *J. Food Drug Anal.*, 2019, **27**, 657–670.
88 N. Struß, J. Bauersachs, T. Welte and J. M. Hohlfeld, *Herz*, 2019, **44**, 477–482.
89 C. Kellerer, K. Kahnert, F. C. Trudzinski, J. Lutter, K. Berschneider, T. Speicher, H. Watz, R. Bals, T. Welte, C. F. Vogelmeier, R. A. Jörres and P. Alter, *Respir. Med.*, 2021, **185**, 106461.
90 J. M. Hohlfeld, J. Vogel-Claussen, H. Biller, D. Berliner, K. Berschneider, H. C. Tillmann, S. Hiltl, J. Bauersachs and T. Welte, *Lancet Respir. Med.*, 2018, **6**, 368–378.
91 E. Menchi, C. El Khattabi, S. Pochet, O. Denis, K. Amighi and N. Wauthoz, *Pharmaceuticals*, 2022, **15**, 963.
92 Y. Yu, B. Fang, X. D. Yang and Y. Zheng, *Front. Pharmacol*, 2023, **14**, 1185076.
93 A. Nanda, A. P. Baptist, R. Divekar, N. Parikh, J. S. Seggev, J. S. Yusin and S. N. Nyenhuis, *J. Asthma*, 2020, **57**, 241–252.
94 C. A. C. Coupland, T. Hill, T. Dening, R. Morriss, M. Moore and J. Hippisley-Cox, *JAMA Intern. Med.*, 2019, **179**, 1084–1093.
95 J. López-Álvarez, J. Sevilla-Llewellyn-Jones and L. Agüera-Ortiz, *Front. Neurosci.*, 2019, **13**, 1309.
96 E. Kose, T. Hirai, T. Seki, S. Hidaka and T. Hamamoto, *J. Clin. Pharm. Therapeut.*, 2018, **43**, 799–806.
97 W. Zhang, X. Feng, J. Yi, Y. Niu and L. Xu, *J. Electroanal. Chem.*, 2019, **842**, 24–33.
98 K. A. Kaczmarek, R. L. Clifford and A. J. Knox, *Chest*, 2019, **155**, 816–824.
99 L. M. Montaño, B. Sommer, J. C. Gomez-Verjan, G. S. Morales-Paoli, G. L. Ramírez-Salinas, H. Solís-Chagoyán, Z. A. Sanchez-Florentino, E. Calixto, G. E. Pérez-Figueroa, R. Carter, R. Jaimez-Melgoza, B. S. Romero-Martínez and E. Flores-Soto, *Int. J. Mol. Sci.*, 2022, **23**, 4167.
100 L. M. Novena, S. Athimoolam, R. Anitha and S. A. Bahadur, *J. Mol. Struct.*, 2022, **1249**, 131585.
101 R. Rolta, D. Salaria, B. Sharma, O. Awofisayo, O. A. Fadare, S. Sharma, C. N. Patel, V. Kumar, A. Sourirajan, D. J. Baumler and K. Dev, *Curr. Pharmacol. Rep.*, 2022, **8**, 149–170.
102 S. Kesavan, N. S. K. Gowthaman, S. Alwarappan and S. A. John, *Sens. Actuators, B*, 2019, **278**, 46–54.
103 T. Wang, E. P. Randviir and C. E. Banks, *Analyst*, 2014, **139**, 2000–2003.
104 P. K. Jiwanti, A. P. Sari, S. Wafiroh, Y. W. Hartati, J. Gunlazuardi, Y. M. T. A. Putri, T. Kondo and Q. K. Anjani, *Sensors*, 2023, **23**, 8597.
105 M. M. Shanbhag, G. Manasa, R. J. Mascarenhas, K. Mondal and N. P. Shetti, *Chem. Eng. J. Adv.*, 2023, **16**, 100516.
106 V. Naresh and N. Lee, *Sensors*, 2021, **21**, 1109.
107 W. Yu, L. Sisi, Y. Haiyan and L. Jie, *RSC Adv.*, 2020, **10**, 15328–15345.
108 F. Bergaya and G. Lagaly, in *Developments in Clay Science*, ed. F. Bergaya and G. Lagaly, Elsevier, 2013, vol. 5, pp. 1–19.
109 A. N. Ghadge and M. M. Ghangrekar, *Electrochim. Acta*, 2015, **166**, 320–328.
110 L. S. Killedar, M. M. Shanbhag, N. P. Shetti, S. J. Malode, R. S. Veerapur and K. Raghava Reddy, *Microchem. J.*, 2021, **165**, 106115.
111 M. M. Shanbhag, N. P. Shetti, S. J. Malode, R. S. Veerapur and K. R. Reddy, *FlatChem*, 2021, **28**, 100255.
112 M. Faried, K. Suga, Y. Okamoto, K. Shameli, M. Miyake and H. Umakoshi, *ACS Omega*, 2019, **4**, 13687–13695.
113 V. B. Patil, S. J. Malode, S. N. Mangasuli, S. M. Tuwar, K. Mondal and N. P. Shetti, *Micromachines*, 2022, **13**, 1166.
114 S. Pourbeyram, J. Abdollahpour and M. Soltanpour, *Mater. Sci. Eng. C*, 2019, **94**, 850–857.
115 T. W. Chen, S. Chinnapaiyan, S. M. Chen, A. Hossam Mahmoud, M. S. Elshikh, H. Ebaid and M. Taha Yassin, *Ultrason. Sonochem.*, 2020, **62**, 104872.
116 D. Zhao, X. Zhang, W. Wang, L. Sui, C. Guo, Y. Xu, X. Zhou, X. Cheng, S. Gao and L. Huo, *Sens. Actuators, B*, 2022, **370**, 132423.
117 M. H. Ghanbari, Z. Norouzi and B. J. M. Etzold, *Microchem. J.*, 2023, **191**, 108836.
118 M. H. Ghanbari, Z. Norouzi and M. M. Ghanbari, *Microchem. J.*, 2020, **156**, 104994.
119 M. H. Ghanbari, M. H. Mashhadizadeh and Z. Norouzi, *J. Iran. Chem. Soc.*, 2021, **18**, 1329–1341.

120 J. B. He, F. Qi, Y. Wang and N. Deng, *Sens. Actuators, B*, 2010, **145**, 480–487.
121 P. Meenakshi, R. Karthick, M. Selvaraj and S. Ramu, *Sol. Energy Mater. Sol. Cells*, 2014, **128**, 264–269.
122 M. Hamidi and K. Zarei, *Russ. Chem. Bull.*, 2020, **69**, 2107–2112.
123 K. Zarei and H. Helli, *J. Electroanal. Chem.*, 2015, **749**, 10–15.
124 S. Anandhakumar and J. Mathiyarasu, *Microchim. Acta*, 2013, **180**, 1065–1071.
125 Y. Li, S. Wu, P. Luo, J. Liu, G. Song, K. Zhang and B. Ye, *Anal. Sci.*, 2012, **28**, 497–502.
126 L. Zhang, T. Wang, X. Fan, D. Deng, Y. Li, X. Yan and L. Luo, *Int. J. Electrochem. Sci.*, 2021, **16**, 21041.
127 M. A. Raj and S. A. John, *J. Phys. Chem. C*, 2013, **117**, 4326–4335.
128 H. L. Guo, X. F. Wang, Q. Y. Qian, F. Bin Wang and X. H. Xia, *ACS Nano*, 2009, **3**, 2653–2659.
129 Y. Z. Zhou, L. J. Zhang, S. L. Chen, S. Y. Dong and X. H. Zheng, *Chin. Chem. Lett.*, 2009, **20**, 217–220.
130 Y. Wang, Y. Ding, L. Li and P. Hu, *Talanta*, 2018, **178**, 449–457.
131 J. C. Kilele, R. Chokkareddy, N. Rono and G. G. Redhi, *J. Taiwan Inst. Chem. Eng.*, 2020, **111**, 228–238.
132 W. Da Silva, M. E. Ghica and C. M. A. Brett, *Anal. Methods*, 2018, **10**, 5634–5642.
133 N. A. Bohari, S. Siddiquee, S. Saallah, M. Misson and S. E. Arshad, *Sensors*, 2020, **20**, 6502.
134 S. Wang, M. Pan, K. Liu, X. Xie, J. Yang, L. Hong and S. Wang, *Food Chem.*, 2022, **381**, 132225.
135 Q. Palomar, X. X. Xu, C. Gondran, M. Holzinger, S. Cosnier and Z. Zhang, *Microchim. Acta*, 2020, **187**, 363.
136 T. Iranmanesh, S. Jahani, M. M. Foroughi, M. S. Zandi and H. Hassani Nadiki, *Anal. Methods*, 2020, **12**, 4319–4326.
137 W. Nowicki, Z. S. Piskuła, P. Kuźma and P. Kirszensztejn, *J. Sol-Gel Sci. Technol.*, 2017, **82**, 574–580.
138 J. Gallego, G. Sierra, F. Mondragon, J. Barrault and C. Batiot-Dupeyrat, *Appl. Catal., A*, 2011, **397**, 73–81.
139 Ç. C. Koçak, A. Nas, H. Kantekin and Z. Dursun, *Talanta*, 2018, **184**, 452–460.
140 S. A. Rezvani and A. Soleymanpour, *Microchem. J.*, 2019, **149**, 104005.
141 Z. Zhou, B. Kong, C. Yu, X. Shi, M. Wang, W. Liu, Y. Sun, Y. Zhang, H. Yang and S. Yang, *Sci. Rep.*, 2014, **4**, 3653.
142 M. Ahsan, M. Z. Ahmad, T. Tesfamichael, J. Bell, W. Wlodarski and N. Motta, *Sens. Actuators, B*, 2012, **173**, 789–796.
143 J. Qin, M. Cao, N. Li and C. Hu, *J. Mater. Chem.*, 2011, **21**, 17167–17174.
144 N. P. Shetti, S. D. Bukkitgar, K. R. Reddy, C. V. Reddy and T. M. Aminabhavi, *Biosens. Bioelectron.*, 2019, **141**, 111417.
145 S. D. Bukkitgar, N. P. Shetti, R. M. Kulkarni, K. R. Reddy, S. S. Shukla, V. S. Saji and T. M. Aminabhavi, *J. Electrochem. Soc.*, 2019, **166**, B3072–B3078.
146 M. H. Ghanbari, A. Khoshroo, H. Sobati, M. R. Ganjali, M. Rahimi-Nasrabadi and F. Ahmadi, *Microchem. J.*, 2019, **147**, 198–206.
147 R. Chokkareddy, N. K. Bhajanthri, G. G. Redhi and D. G. Redhi, *Curr. Anal. Chem.*, 2018, **14**, 391–398.
148 K. Turcheniuk and V. N. Mochalin, *Nanotechnology*, 2017, **28**, 252001.
149 P. K. Jiwanti, B. Y. Wardhana, L. G. Sutanto, D. M. M. Dewi, I. Z. D. Putri and I. N. I. Savitri, *Molecules*, 2022, **27**, 7578.
150 Y. Einaga, *Bull. Chem. Soc. Jpn.*, 2018, **91**, 1752–1762.
151 Y. Einaga, *J. Appl. Electrochem.*, 2010, **40**, 1807–1816.
152 D. Dragoe, N. Spătaru, R. Kawasaki, A. Manivannan, T. Spătaru, D. A. Tryk and A. Fujishima, *Electrochim. Acta*, 2006, **51**, 2437–2441.
153 K. Cinková, N. Zbojeková, M. Vojs, M. Marton, A. Samphao and Ľ. Švorc, *Anal. Methods*, 2015, **7**, 6755–6763.
154 P. K. Jiwanti, A. P. Sari, S. Wafiroh, Y. W. Hartati, J. Gunlazuardi, Y. M. T. A. Putri, T. Kondo and Q. K. Anjani, *Sensors*, 2023, **23**, 8597.
155 P. Di Matteo, A. Trani, M. Bortolami, M. Feroci, R. Petrucci and A. Curulli, *Sensors*, 2023, **23**, 7731.
156 S. D. Bukkitgar and N. P. Shetti, *Mater. Today: Proc.*, 2018, **5**, 21474–21481.
157 R. D. Crapnell and C. E. Banks, *Talanta*, 2021, **3**, 100037.
158 Z. Wang, R. An, Y. Dai and H. Luo, *Int. J. Electrochem. Sci.*, 2021, **16**, 210450.
159 M. Ghalkhani, E. M. Khosrowshahi and E. Sohouli, in *Handbook of Carbon-Based Nanomaterials*, ed. S. Thomas, C. Sarathchandran, S. A. Ilangovan and J. C. Moreno-Piraján, Elsevier, 2021, pp. 159–207.
160 J. Bartelmess and S. Giordani, *Beilstein J. Nanotechnol.*, 2014, **5**, 1980–1998.
161 R. An, W. Kuang, Z. Li, T. Mu and H. Luo, *Processes*, 2023, **11**, 2547.
162 Y. Duan, A. Wang, Y. Ding, L. Li, D. Duan, J. Lin, C. Yu and J. Liu, *J. Pharm. Biomed. Anal.*, 2021, **192**, 113663.
163 P. Karpagavinayagam, R. Baby Suneetha, C. Vedhi and J. Antory Rajam, in *Carbon Nanomaterials-Based Sensors: Emerging Research Trends in Devices and Applications*, ed. J. G. Manjunatha and C. M. Hussain, Elsevier, 2022, pp. 417–428.
164 M. Zhi, A. Manivannan, F. Meng and N. Wu, *J. Power Sources*, 2012, **208**, 345–353.
165 B. J. Sanghavi and A. K. Srivastava, *Electrochim. Acta*, 2010, **55**, 8638–8648.
166 I. Švancara, K. Kalcher, A. Walcarius and K. Vytřas, *Electroanalysis with Carbon Paste Electrodes*, 2012, pp. 1–666.
167 R. A. Al-Haidari, N. A. Abdallah, M. M. Al-Oqail, E. S. Al-Sheddi, S. M. Al-Massarani and N. N. Farshori, *Inorg. Chem. Commun.*, 2020, **119**, 108080.
168 G. J. Yang, K. Wang, J. J. Xu and H. Y. Chen, *Anal. Lett.*, 2004, **37**, 629–643.
169 R. Emamian, M. Ebrahimi and H. Karimi-Maleh, *J. Electrochem. Soc.*, 2018, **165**, B762–B766.
170 H. Beitollahi, K. Movlaee, M. R. Ganjali and P. Norouzi, *J. Electroanal. Chem.*, 2017, **799**, 576–582.
171 A. K. Attia, M. A. Al-Ghobashy, G. M. El-Sayed and S. M. Kamal, *Data Brief*, 2018, **21**, 150–153.
172 X. Teng, J. Li, Z. Wang, Z. Wei, C. Chen, K. Du, C. Zhao, G. Yang and Y. Li, *RSC Adv.*, 2020, **10**, 24712–24720.